# Cingulin is dispensable for epithelial barrier function and tight junction structure, and plays a role in the control of claudin-2 expression and response to duodenal mucosa injury

**Laurent Guillemot[1], Yann Schneider[1], Paola Brun[2], Ignazio Castagliuolo[2], Daniela Pizzuti[2], Diego Martines[3], Lionel Jond[1], Massimo Bongiovanni[4] and Sandra Citi[1,5,*]**

[1]Department of Molecular Biology, and [5]Department of Cell Biology, University of Geneva, CH-1211 Geneva, Switzerland
[2]Department of Histology, University of Padova, 35100 Padova, Italy
[3]Department of Gastroenterology, University of Padova, 35100 Padova, Italy
[4]Institute of Pathology, CH-6601 Locarno, Switzerland
*Author for correspondence (sandra.citi@unige.ch)

*Accepted 30 July 2012*
*Journal of Cell Science 125, 5005–5014*

*doi: 10.1242/jcs.101261*

## Summary

Cingulin (CGN) is a 140 kDa protein, which is localized to the cytoplasmic region of vertebrate tight junctions (TJ), and regulates gene expression and RhoA signaling in cultured cells. To investigate the function of CGN at the organism level, we generated CGN knockout ($CGN^{-/-}$) mice by homologous recombination. $CGN^{-/-}$ mice are viable and fertile, and are born at the expected mendelian ratios. Immunohistochemistry, immunofluorescence, electron microscopy and permeability assays of epithelial tissues of $CGN^{-/-}$ mice show no cingulin labeling at junctions, a normal localization of TJ proteins, and normal TJ structure and barrier function. Microarray analysis of intestinal cells does not show significant changes in gene expression between $CGN^{-/-}$ and $CGN^{+/+}$ mice, whereas immunoblotting analysis shows a twofold increase in the levels of claudin-2 protein in the duodenum and the kidney of $CGN^{-/-}$ mice, compared to $CGN^{+/+}$ littermates. Furthermore, $CGN^{-/-}$ mice show an exacerbated response to the ulcerogenic action of cysteamine, whereas acute injury of the colon by dextran sodium sulfate elicits undistinguishable responses in $CGN^{-/-}$ and $CGN^{+/+}$ mice. We conclude that at the organism level cingulin is dispensable for the structure and barrier function of TJ, and is embedded in signaling networks that control the expression of claudin-2, and the mucosal response to acute injury in the duodenum.

**Key words:** Cingulin, Claudin-2, Mouse, Tight junctions, ZO-1, Occludin, RhoA

## Introduction

Vertebrate epithelial cells display a characteristic apicolateral junctional complex, comprising tight junctions (TJ) and adherens junctions. TJ are primarily responsible for the permeability barrier function of epithelial tissues, and for maintaining the apicobasal polarity of epithelial cells (Shin et al., 2006; Van Itallie and Anderson, 2006). In addition, TJ play important roles in control of signaling, cell differentiation, and gene expression (Guillemot et al., 2008b; McCrea et al., 2009). The barrier function of TJ is of critical importance in the physiology of major epithelial organs, including the kidney and the intestine, where compositionally distinct extracellular compartments must be generated and maintained. The disruption of the normal barrier function of epithelia has been implicated in the pathogenesis of human diseases, including inflammatory bowel disease (Schmitz et al., 1999), and magnesium wasting syndrome (Simon et al., 1999).

Barrier and signaling functions of TJ are orchestrated by a complex network of transmembrane and cytoplasmic proteins. Claudins, a family of proteins that comprises ~25 isoforms, regulate the tissue-specific charge- and size-selective permeability of TJ to ions (Tsukita and Furuse, 2000; Van Itallie and Anderson, 2006). Claudin-2 is typical of 'leaky' epithelia, and increases permeability to cations, when ectopically expressed in cells that normally lack it (Furuse et al., 2001; Amasheh et al., 2002). The protein complexes in the cytoplasmic region of TJ are of critical importance in the control of TJ barrier function, since they form a scaffold for claudins and other TJ membrane proteins, and they link membrane proteins to the cytoskeleton, thus regulating junction architecture and barrier function (Mitic and Anderson, 1998; Turner, 2000; Guillemot et al., 2008b). The cytoplasmic region of TJ also contains proteins which contribute to the establishment of polarity, to the regulation of transcription and translation, and to the regulation of the Rho family GTPases (reviewed in Shin et al., 2006; Guillemot et al., 2008b; McCrea et al., 2009; Citi et al., 2011).

Cingulin (CGN; from the Latin *cingere* to form a belt around) is a 140 kDa protein, which is specifically localized in the cytoplasm underlying the TJ (Citi et al., 1988; Citi et al., 1989). CGN exists as a dimer, each subunit comprising globular domains (head and tail), and a central α-helical coiled-coil domain (rod) (Cordenonsi et al., 1999). CGN interacts with

several cytoplasmic TJ proteins, including ZO-1, ZO-2 and ZO-3, as well as with actin and myosin (Cordenonsi et al., 1999; D'Atri et al., 2002). The head domain of CGN is required for CGN recruitment to junctions, primarily via its interaction with ZO-1 (Cordenonsi et al., 1999; D'Atri et al., 2002). To clarify the function of CGN, we previously generated embryonic stem (ES) cells in which the CGN locus was targeted by homologous recombination, to delete the head domain (Guillemot et al., 2004). In epithelial cells obtained by differentiation of $CGN^{-/-}$ ES cells into embryoid bodies (EB), TJ were devoid of CGN, and had normal ultrastructure, localization of other TJ proteins, and barrier function. However, CGN targeting resulted in differentiation-dependent changes in the expression of a large number of genes, including transcription factors, and TJ protein genes, namely claudin-2, claudin-6, claudin-7 and occludin (Guillemot et al., 2004; Citi et al., 2009). Significantly, cingulin depletion in MDCK cells also resulted in increased expression of claudin-2 (Guillemot and Citi, 2006), suggesting that CGN is part of a signaling network that controls claudin-2 expression in different cell culture model systems. In addition, CGN controls RhoA activity in cultured epithelial cells, through its interaction with the RhoA activator GEF-H1, and cingulin depletion results in increased cell proliferation in MDCK cells (Aijaz et al., 2005; Guillemot and Citi, 2006; Citi et al., 2009).

Here we investigate the physiological role of CGN in a whole organism, by targeting CGN in mice, and analyzing the phenotype of $CGN^{-/-}$ mice. Our results provide conclusive evidence that CGN is dispensable for TJ barrier function and organization in epithelial tissues *in vivo*, and indicate that CGN is involved in signaling networks that control claudin-2 expression in kidney and duodenum, and in the response to acute mucosal injury in the duodenum.

## Results

### Targeting of the cingulin locus and generation of $CGN^{-/-}$ mice

To study the function of CGN at the organism level, we generated mice lacking junctional CGN, by targeting the CGN locus in embryonic stem cells. The mouse CGN locus comprises 20 exons, spanning ~27 kb of genomic sequence. The CGN targeting vector was designed to insert within the CGN locus three LoxP sites, one upstream and two downstream of Exon 1, flanking the Neo resistance cassette (Fig. 1A, targeting vector). exon 1 contains the putative ATG, and codes for most of the globular head domain, which is required for junctional recruitment of cingulin. The correct integration of the targeting vector was determined by Southern blot analysis of genomic DNA isolated from clones of embryonic stem cells (Fig. 1B). Positive embryonic stem cell clones were injected into C57BL/6 blastocysts, and chimeras were mated to C57BL/6 strain, to produce the heterozygote F1 mouse generation. To obtain the mutated knockout (KO) allele, heterozygous F1 mice were mated to mice expressing the Cre recombinase. The resulting mosaic offspring was mated to the WT C57BL/6 strain, and the progeny was genotyped, to select mice in which Cre-mediated recombination occurred between the first and third LoxP sites (Fig. 1A, mutated allele), resulting in the deletion of exon 1 and the Neo cassette. Primer sets located both within and outside the deleted region were used for genotyping (Fig. 1C).

$CGN^{-/-}$ mice were born at the expected mendelian ratios (Table 1), had normal weight at birth, developed normally, and showed normal appearance, behavior and fertility.

### Normal intestinal histology and TJ structure, and lack of cingulin in the junctions of epithelial cells in $CGN^{-/-}$ mice

We examined the gross anatomy and histology of major organs, including heart, lung, kidney, liver, intestine, pancreas, spleen, and

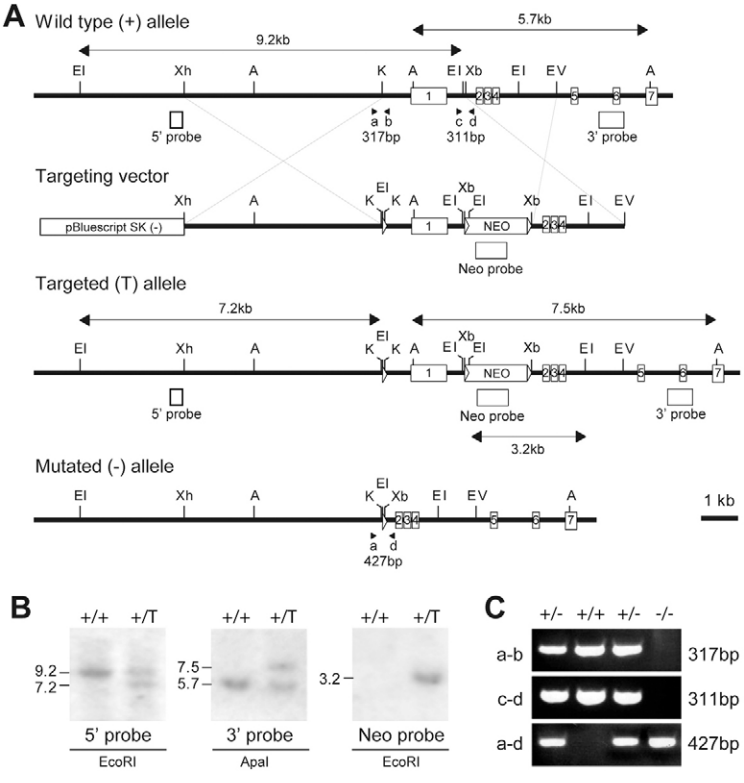


**Fig. 1. Targeting the gene locus by homologous recombination.** (**A**) Schematic diagrams representing the wild-type allele (+), the targeting vector, the targeted (T) allele, and the mutated (−) allele. The position of the 5′ and 3′ probes, the Neo probe, and the PCR primers (a, b, c, d) used for genotyping are indicated below the diagrams. Exons are indicated by boxed numbers. Restriction sites (EI, *Eco*RI; Xh, *Xho*I; A, *Apa*I; K, *Kpn*I; Xb, *Xba*I; EV, *Eco*RV), as well as position and size of fragments generated by digestion are indicated above (for 5′ and 3′ probes) and below (for the Neo probe) the diagrams. The targeting vector comprises a 7.6 kb left arm containing a LoxP (▷) site (cloned into a *Kpn*I site), a neomycin resistance cassette (NEO) cloned between exons 1 and 2 and flanked by LoxP sites, and a 2.4 kb right arm, comprising exons 2, 3 and 4. Exon 1 codes for residues 1–279 of the mouse cingulin protein sequence (e.g. most of the 334-residue long head domain). Cre-mediated recombination between the first LoxP site (upstream of exon 1) and the third LoxP site (at the 3′ end of the Neo cassette) results in the formation of the mutated (−) allele. (**B**) Southern blot analysis of *Eco*RI-digested genomic DNA with the 5′ probe results in a 9.2 kb fragment in the wild-type allele, and a 7.2 kb fragment in the targeted allele, due to the insertion of an *Eco*RI site flanking the first LoxP site. Southern blot analysis of *Apa*I-digested genomic DNA with the 3′ probe results in a 5.7 kb fragment in the wild-type allele, and a 7.5 kb fragment in the targeted allele, due to the insertion of the Neo cassette. Southern blot analysis of *Eco*RI-digested genomic DNA with the Neo probe results in a 3.2 kb fragment in the targeted allele. (**C**) PCR amplification of genomic DNA from tail clippings using primer sets 'a–b' and 'c–d' generates fragment of 317 bp and 311 bp, respectively, in the WT allele, and no product in the mutated allele. PCR amplification using primer sets a–d generates a fragment of 427 bp in the mutated allele.

**Table 1. Genotype of offsping from mating of heterozygous CGN mice**

| Genotype | No. of mice | (%) |
|---|---|---|
| +/+ | 165 | (26) |
| +/− | 298 | (48) |
| −/− | 164 | (26) |

skin, and did not detect any abnormalities. For example in the duodenum and the ileum, a normal morphology of villi and crypts, and a normal organization of the intestinal epithelium was observed (Fig. 2A,B). Ultrastructural analysis of thin sections of duodenum by transmission electron microscopy showed the presence of typical apical TJ in the tissue of $CGN^{-/-}$ mice, which were morphologically indistinguishable from the TJ of $CGN^{+/+}$ mice (Fig. 2C,D). Immunohistochemical analysis of the duodenum of $CGN^{+/+}$ mice showed the localization of CGN along the apical junctional regions of polarized epithelial cells (Fig. 2E; and magnified inset). In contrast, sections of duodenum from $CGN^{-/-}$ littermates showed no detectable CGN signal in corresponding regions (Fig. 2F; and magnified inset). Immunohistochemistry and immunofluorescence analysis of sections of epithelial tissues and organs, including the kidney, the colon and the liver were carried out using antibodies against CGN and different TJ proteins (supplementary material Fig. S1). No junctional CGN labeling was detected in cells of any epithelial tissue that we examined from $CGN^{-/-}$ mice, whereas the localization of paracingulin, claudin-1, claudin-7, occludin, ZO-1, and claudin-5 was indistinguishable in tissues from $CGN^{+/+}$ and $CGN^{-/-}$ littermates (supplementary material Fig. S1). Taken together, these observations demonstrate that our targeting approach results in epithelial tissues with cell-cell junctions devoid of CGN, and that the lack of CGN does not detectably alter the structure and molecular composition of TJ, in agreement with previous observations using cultured cell models (Guillemot et al., 2004; Guillemot and Citi, 2006).

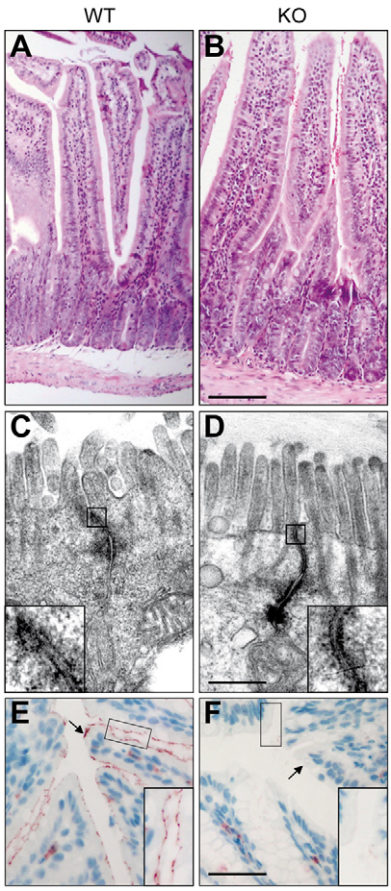


**Fig. 2. Normal epithelial histology and TJ, and no detectable cingulin immunolabeling in the intestine of $CGN^{-/-}$ mice.** (**A**,**B**) Hematoxylin- and Eosin-stained histological section of duodenum from WT (A) and KO (B) mice. No abnormality was detected in KO tissue. (**C**,**D**) Transmission electron micrograph of ultrathin sections of duodenum from WT (C) and KO (D) mice. The ultrastructure of TJ (magnified insets) in KO tissue did not reveal significant changes with respect to WT. (**E**,**F**) Immunohistochemical localization of CGN in duodenum from WT (E) and KO (F) mice. Cingulin labeling is detected along the apical borders of intestinal epithelial cells in WT (E), but not in KO (F) tissue (arrows and magnified insets). Scale bars: 50 μm (A,B), 200 nm (C,D), 30 μm (E,F).

### Expression of TJ protein genes in cingulin KO mice

Previously, we showed that the targeted inactivation of CGN in differentiated mouse embryoid bodies resulted in changes in the expression of many genes, including increases in the mRNA levels of claudin-2 (about 20-fold), claudin-6 (about twofold), claudin-7 (about fourfold) and occludin (about threefold) (Guillemot et al., 2004). Furthermore, CGN depletion in kidney epithelial (MDCK) cells resulted in increased mRNA levels of claudin-2 (about threefold) (Guillemot and Citi, 2006). To test whether changes in gene expression occur in tissues of $CGN^{-/-}$ mice, we first carried out a microarray analysis on RNA isolated from intestinal epithelial cells. In a comparison involving over 46,600 genes, there was no statistically significant change in gene expression, above random background noise (Fig. 3A). Next, we isolated RNA from liver, kidney and intestinal tissues, and examined by qRT-PCR the expression of a selected group of TJ protein genes in couples of $CGN^{+/+}$ and $CGN^{-/-}$ littermates (Fig. 3B–D). In each pair, the measured levels of expression of each mRNA in the WT sample was taken as 100%, and the levels of mRNA in the KO sample were expressed as percent of WT. In agreement with the results of the microarray analysis, we did not find statistically significant differences in the levels of mRNA coding for ZO-3, claudin-2, claudin-6, claudin-7 and occludin, between $CGN^{+/+}$ and $CGN^{-/-}$ littermates (Fig. 3B–D). Although in some cases, for example for claudin-6 and claudin-7, the mRNA levels were higher in KO tissues, the increase was not statistically significant, probably due to heterogeneity of samples, and variability in levels of expression. Paracingulin and ZO-1, that form a complex with cingulin (D'Atri et al., 2002; Paschoud et al., 2011), also did not show altered levels of mRNA expression (Fig. 3B–D). The levels of the same genes in additional tissues (spleen, colon, ileum) that we examined were also unchanged (data not shown).

### Claudin-2 protein expression is increased in the duodenum and kidney of $CGN^{-/-}$ mice

In addition to changes in transcript levels, we previously observed changes in protein levels of specific TJ proteins in $CGN^{-/-}$ embryoid bodies (Guillemot et al., 2004) and CGN-depleted MDCK cells (Guillemot and Citi, 2006). To investigate whether changes in the expression levels of these TJ proteins occur in $CGN^{-/-}$ mice, lysates were prepared from kidney, liver,

and epithelial cells from three different segments of the intestine (duodenum, ileum and colon). Optimal lysis conditions were established for each tissue, and lysates were carefully normalized for total protein content, using anti-tubulin antibodies (Fig. 4A).

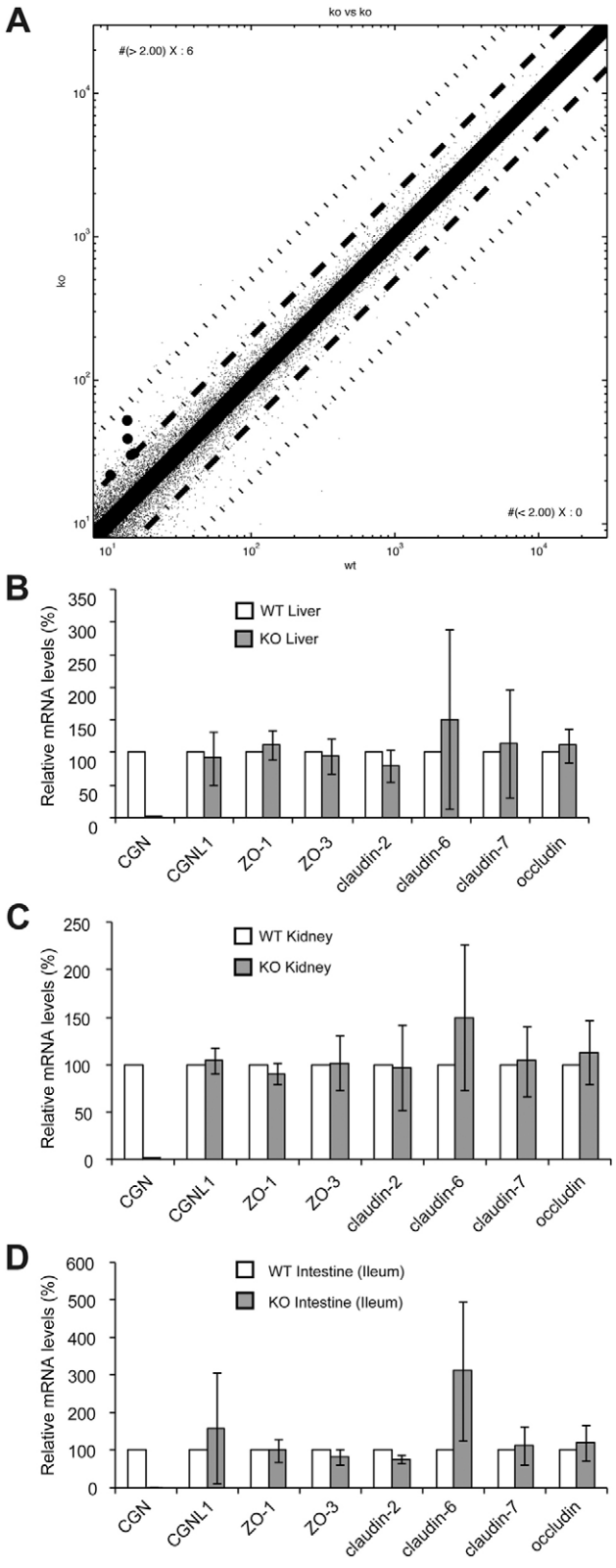


Immunoblotting analysis with anti-CGN antibodies detected the 140 kDa CGN polypeptide in lysates of $CGN^{+/+}$, but not $CGN^{-/-}$ mice, demonstrating that our targeting approach successfully disrupted the CGN gene (Fig. 4A). A truncated protein containing the rod-tail domains, was detected in lysates of $CGN^{-/-}$ mouse tissues (not shown, see Guillemot et al., 2004), but this is functionally irrelevant, since (1) this truncated form does not target to junctions (Fig. 2), where CGN is active (Cordenonsi et al., 1999; Guillemot et al., 2004), (2) overexpression of the rod–tail domain in epithelial cells gives no phenotype (Paschoud and Citi, 2008), and (3) the rod–tail domain does not rescue the phenotype of CGN-depleted cells (Guillemot and Citi, 2006) (L.G., and S.C., unpublished data). Paracingulin and ZO-1 proteins were expressed at barely detectable levels in duodenum and ileum samples, suggesting a rostro-caudal gradient of increasing expression along the intestinal tract (Fig. 4A). No significant changes in their relative levels of expression were detected in $CGN^{+/+}$ and $CGN^{-/-}$ littermates, similarly to what observed for ZO-3 and occludin (Fig. 4A). In contrast, claudin-2 levels of expression were increased by about twofold, only in kidney and duodenum from $CGN^{-/-}$ mice, when compared to $CGN^{+/+}$ littermates (Fig. 4A,B). The increased expression of the claudin-2 protein in kidney and duodenum tissues did not result in any detectable changes in the pattern of tissue distribution, subcellular localization, and intensity of labeling of claudin-2, as determined by immunocytochemical analysis of tissue sections (Fig. 5). Immunoblotting of mouse tissue lysates with different antibodies against claudin-6, claudin-7, and other claudin isoforms was attempted, but gave weak or no labeling of specific polypeptides.

Since in MDCK cells the upregulation of claudin-2 expression was dependent on increased RhoA activation (Guillemot and Citi, 2006), we measured the levels of active RhoA in the kidney and duodenum from $CGN^{-/-}$ and $CGN^{+/+}$ littermates, using a pulldown assay. Immunoblotting showed low amounts of active RhoA in lysates of mouse tissues, compared to lysates of MDCK cells, and the levels of active RhoA were not significantly different when comparing lysates from $CGN^{+/+}$and $CGN^{-/-}$ tissues (Fig. 4C).

**Fig. 3. Expression of TJ protein genes in the liver, kidney, and intestine of $CGN^{-/-}$ mice is not significantly different from the expression in $CGN^{+/+}$ mice.** (**A**) Dot-plot analysis of the normalized expression levels (expressed in arbitrary units) of the 46,664 mouse transcripts, comparing transcripts in KO (*y*-axis) and WT (*x*-axis) samples. The lines parallel to the central line represent the cutoff limits of 1.5- and 5-fold change in expression. We found 367 probes with a *P*-value $<0.05$, including 12 (Plin, Poldip3, Pias3, Epb4.1, Pogz, Taf3, Gcnt2, Atxn10, B930014J03Rik, Frs3, A930023F12Rik, Cpa1) with a fold change (increase or decrease) $>2$. However by false discovery rate (FDR) analysis we found only two probes (Gm9934, fold change 1.2, and Tnfsrf22, fold change 1.6). Moreover, these are not significant, since power analysis using the Partek Genomics Suite shows that we are not able to detect fold changes below 2.0 using triplicate samples. Therefore, considering the number of transcripts that were analyzed, these can be considered as random events. (**B–D**) Histograms showing the relative mRNA levels (determined by qRT-PCR, and taking the value of WT tissue as 100%) for the indicated TJ proteins, in liver (B), kidney (C), and intestinal (D) tissues from WT (white bars) and KO (gray bars) littermates. The values represent the average percentage based on $n=6$ pairs. None of the differences in mRNA levels were statistically significant ($P<0.05$).

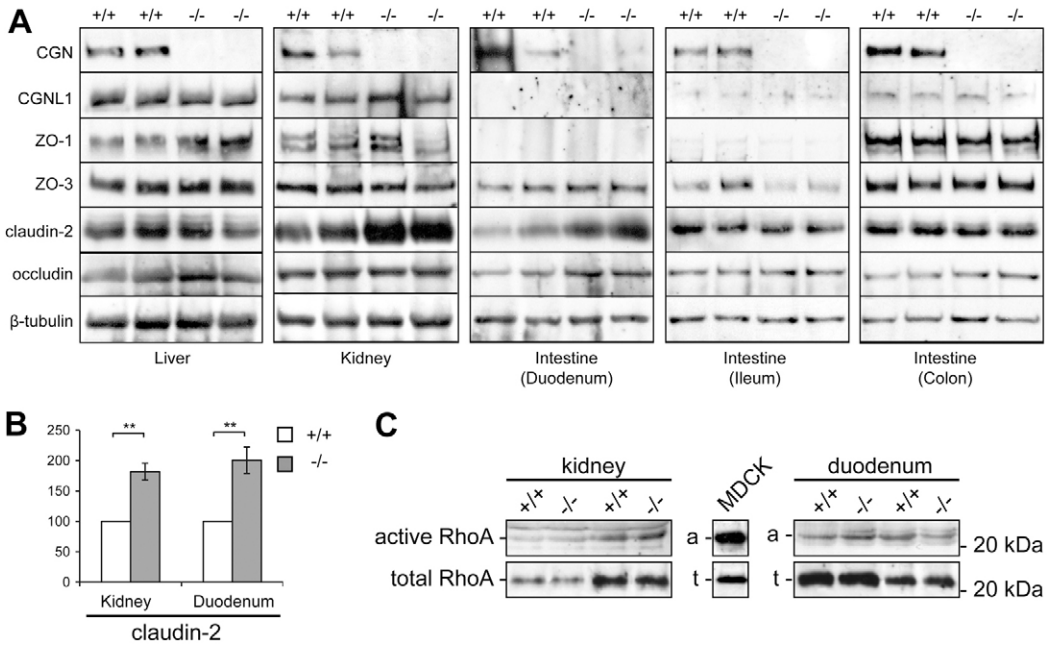


**Fig. 4. Increased levels of claudin-2 protein in the kidney and duodenum of CGN$^{-/-}$ mice.** (**A**) Immunoblot analysis of protein in lysates from the indicated tissues, using antibodies against different TJ proteins (see Materials and Methods). The images show representative examples of blots from two CGN$^{-/-}$ and CGN$^{+/+}$ littermates. Equivalent protein loadings were analyzed and normalized by β-tubulin staining. Note that full-length cingulin is undetectable in CGN$^{-/-}$ lysates. (**B**) Histogram showing a semi-quantitative measurement of the differences in expression of claudin-2 in kidney and duodenum tissues from CGN$^{-/-}$ and CGN$^{+/+}$ littermate pairs ($n=8$). The differences are statistically significant (**$P<0.005$). (**C**) RhoA activity in lysates of kidney and duodenum of CGN$^{-/-}$ and CGN$^{+/+}$ mice, determined by immunoblot analysis of active RhoA isolated by GST pulldown with GST–rhotekin, and total RhoA levels. MDCK cells were used as a positive control for the pulldown assay, with total and activated RhoA samples which were run in the same gel and exposed for the same length of time as the corresponding kidney and duodenum samples.

### Normal intestinal permeability, inflammatory parameters and response to dextran sodium sulfate in CGN$^{-/-}$ mice

Since increased levels of claudin-2 expression has been linked to increased intestinal permeability in inflammatory bowel disease (Zeissig et al., 2007; Weber et al., 2008), we next examined the intestinal barrier function in CGN$^{-/-}$ mice, and the levels of inflammatory cytokines in portal and systemic blood (Brun et al., 2005). Mucosal preparations from either the duodenum or the colon of CGN$^{+/+}$ and CGN$^{-/-}$ littermates were mounted in Ussing chambers, and transepithelial electrical resistance was measured. As shown in Fig. 6A, no statistically significant difference in resistance was detectable when comparing tissues from CGN$^{+/+}$ and CGN$^{-/-}$ mice (Fig. 6A). Portal blood levels of endotoxin and systemic blood levels of TNF-α were not significantly different in CGN$^{+/+}$ and CGN$^{-/-}$ littermates (Fig. 6B). Similarly, additional markers of hepatic and intestinal inflammation, including levels of fibronectin and collagen-I in hepatic stellate cells stimulated by LPS, intestinal myeloperoxidase activity, and intestinal expression of IL-1β and TNF-α were not significantly different between CGN$^{+/+}$ and CGN$^{-/-}$ littermates (supplementary material Fig. S2A). To determine whether the lack of CGN would result in a different sensitivity of the intestinal mucosa to acute inflammatory injury, we challenged the mice with dextran sodium sulfate (DSS), which induces acute colitis, weight loss and diarrhea (Okayasu et al., 1990). Analysis of the pattern of weight loss (Fig. 6C) and measurement of levels of intestinal inflammatory cytokines (supplementary material Fig. S2B,C) showed no significant difference between CGN$^{+/+}$ and CGN$^{-/-}$ littermates.

### CGN$^{-/-}$ mice are more sensitive to the ulcerogenic action of cysteamine

We next used a disease model of acute injury which targets more specifically the duodenum, where increased claudin-2 expression was observed. CGN$^{+/+}$ and CGN$^{-/-}$ mice were challenged with cysteamine hydrochloride, a widely used agent to chemically induce ulcers, and study the effect of different substances on ulcer pathogenesis (Szabo, 1978; Cahill et al., 1986). The duodenum of cysteamine-treated mice was dissected and examined, to assess the presence and number of ulcers, and their severity (ulcer score). These parameters, together with ulcer prevalence, were used to calculate the ulcer index for each mouse (see Materials and Methods). The ulcer index of CGN$^{-/-}$ mice was significantly higher ($P<0.0005$, $n=12$) than that of CGN$^{+/+}$ mice (Fig. 7A), due to an increase in the number, severity and prevalence of ulcers. For example, all of the CGN$^{-/-}$ mice showed ulcer lesions, whereas five out of the twelve CGN$^{+/+}$ mice showed no lesions.

To try to understand the mechanism through which the lack of CGN could influence the response to cysteamine-induced ulcer formation, we first carried out a histopathological analysis of the duodenal mucosa. Superficial and deep located ulcers showed similar histopathological changes in CGN$^{+/+}$ and CGN$^{-/-}$ mice, with necrosis of epithelium and stromal cells, a mild mononuclear infiltrate, and absence of granulation tissue (Fig. 7B,C), suggesting that the greater severity of the ulcer induction in CGN$^{-/-}$ mice was not due to a different inflammatory response. Considering normal mucosa, samples from CGN$^{+/+}$ and CGN$^{-/-}$ mice displayed a similar degree of

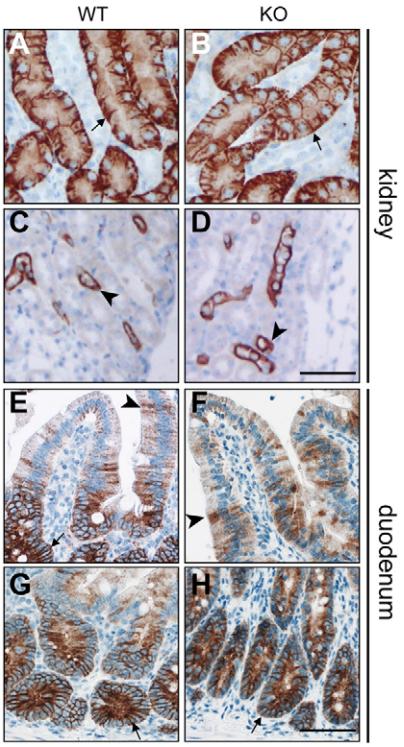


**Fig. 5. The tissue distribution and subcellular localization of claudin-2 in the kidney and duodenum of CGN$^{-/-}$ and CGN$^{+/+}$ mice are similar.** Immunohistochemical localization of claudin-2 in the kidney cortex (**A**,**B**) and medulla (**C**,**D**), and in duodenum crypts (**E**,**F**) and villi (**G**,**H**) of CGN$^{+/+}$ (A,C,E,G) and CGN$^{-/-}$ (B,D,F,H) littermates. Claudin-2 is detected in proximal tubules (arrows) and in the thin descending limb of Henle's loop (Kiuchi-Saishin et al., 2002). In the duodenum, strong labeling for claudin-2 is detected in the crypt proliferative zone at the base of the villi (arrows), and weak labeling is detected in epithelial cells lining the villi (arrowheads) (Rahner et al., 2001). Scale bar: 50 μm.

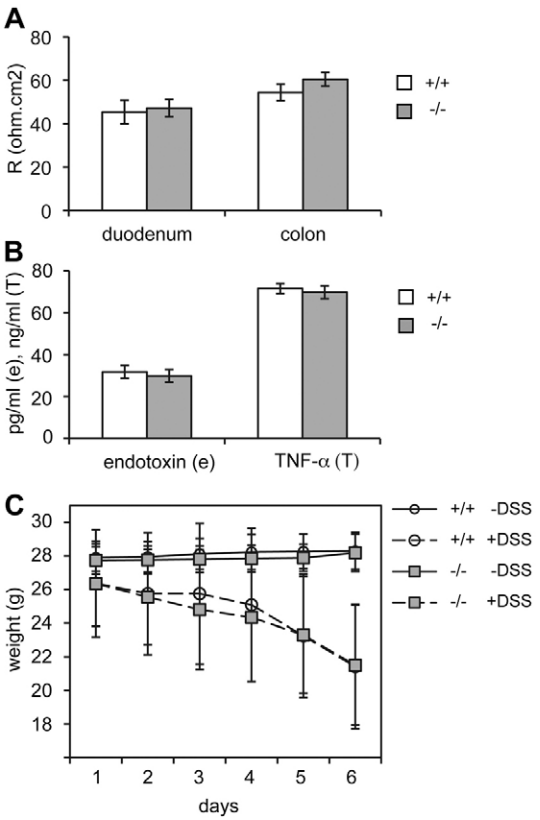


**Fig. 6. CGN$^{-/-}$ mice do not exhibit increased intestinal permeability, inflammation or response to treatment with DSS.** (**A**) Electrical resistance ($R$, ohm/cm$^2$) in duodenum and colon mucosal samples from pairs ($n$=10) of CGN$^{+/+}$ (white bars) and CGN$^{-/-}$ (gray bars) littermates, measured using Ussing chambers. (**B**) Portal endotoxemia and systemic proinflammatory cytokine (TNF-α) levels in pairs ($n$=10) of CGN$^{+/+}$ (white bars) and CGN$^{-/-}$ (gray bars) littermates ($n$=10). (**C**) Assessment of body weight in pairs ($n$=6) of CGN$^{+/+}$ (circles) and CGN$^{-/-}$ (squares) littermates, without (white symbols) and with (gray symbols) DSS treatment. The values were not statistically significantly different between WT and KO.

lymphocytic and plasma cell infiltrate in the lamina propria, with almost complete absence of granulocytes, similar morphology of villi and crypts and a normal crypt/villus ratio (not shown). Next, we asked whether the epithelial cells within the intact mucosa of the duodenum from CGN$^{+/+}$ and CGN$^{-/-}$ mice showed different proliferation rate. To evaluate proliferation, sections were labeled with antibodies against phospho-histone H3, which labels cells in the G2-M phases of the cell cycle. Although the percentage of proliferating cells was slightly higher in the duodenum of CGN$^{-/-}$ mice (Fig. 7D–F), the difference was not statistically significant, suggesting that the different responses of the CGN$^{+/+}$ and CGN$^{-/-}$ mice could not be explained by a difference in proliferating activity. Proliferation was also assessed the colon, and duodenum from untreated mice, and there was no significant differences between CGN$^{+/+}$ and CGN$^{-/-}$ mice (supplementary material Fig. S3), consistent with the absence of hyperplastic or any other detectable histological or macroscopic changes in tissues from CGN$^{-/-}$ mice.

## Discussion

In this study we report the generation and phenotypic characterization of mice lacking the cytoplasmic TJ protein cingulin (CGN). CGN$^{-/-}$ mice are viable, fertile, and do not display detectable histological abnormalities in major epithelial organs, or altered barrier function of the intestinal mucosa. However, CGN$^{-/-}$ mice show increased claudin-2 protein levels in the kidney and the duodenum, providing evidence that CGN is embedded in signaling pathways that regulate the expression of claudin-2 not only in cultured cells, but also in a whole organism. Furthermore, CGN$^{-/-}$ mice show an increased sensitivity to the pathogenic action of the ulcerogenic agent cysteamine.

Gene knockout in mice is a powerful approach to study the role of proteins within the context of a whole vertebrate organism. However, only few mouse knockout models of cytoplasmic TJ proteins have been described. Knockout of afadin/AF-6, PAR-3, ZO-1 and ZO-2 lead to embryonic lethality, indicating an essential role of these proteins in early development, whereas the knockout of ZO-3 has a mild phenotype (Zhadanov et al., 1999; Ikeda et al., 1999; Adachi et al., 2006; Katsuno et al., 2008; Xu et al., 2008; Xu et al., 2009). No previous study has addressed the role of CGN at the whole organism level. Our strategy to generate CGN$^{-/-}$ mice was to obtain a targeted deletion of the CGN head domain, which results in epithelial cells lacking any detectable junctional cingulin. As in the case of CGN mutant embryoid bodies (Guillemot et al., 2004) and CGN-depleted MDCK cells

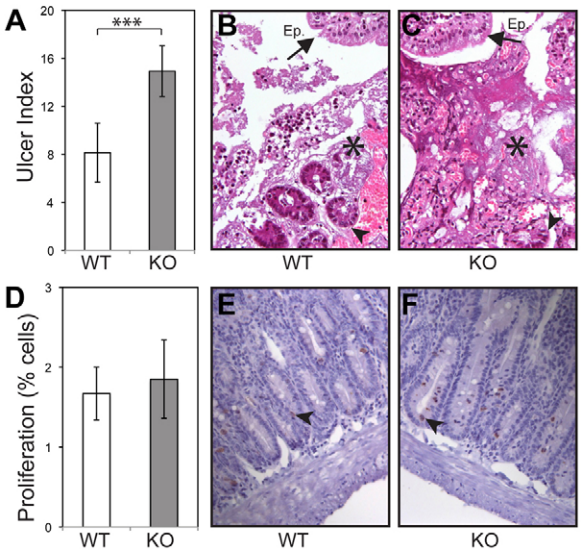


**Fig. 7. Increased ulcerogenic response of CGN$^{-/-}$ duodenum to cysteamine, without increased proliferation.** (**A**) Histogram showing the ulcer index (calculated as described in Materials and Methods) of the duodenum of mice treated with cysteamine, as a function of genotype. The ulcer index is significantly higher (***$P<0.0005$, $n=12$) in the duodenum of CGN$^{-/-}$ mice. (**B**,**C**) Histological images (Hematoxylin and Eosin stained) of duodenal ulcers in CGN$^{+/+}$ (B) and CGN$^{-/-}$ (C) mice. Ep., surface epithelium; asterisk, necrotic areas; arrowheads, crypts. (**D**) Histogram showing cell proliferation (percentage of phospho-histone-H3-positive, mitotic cells) in duodenum sections of cysteamine-treated CGN$^{-/-}$ and CGN$^{+/+}$ mice. (**E**,**F**) Immunohistochemical staining of duodenal epithelium sections from CGN$^{+/+}$ (E) and CGN$^{-/-}$ (F) cysteamine-treated mice, with anti-phospho-histone H3 antibodies. Arrowheads indicate positive, mitotic cells. Original magnification 400×.

(Guillemot and Citi, 2006), we could not detect in CGN$^{-/-}$ epithelial tissues any abnormality in the structure and function of TJ, and the localization of TJ proteins, confirming that CGN is dispensable for TJ structure and function.

Whereas in embryoid bodies we observed significant changes in the expression of many genes, microarray and RT-PCR analyses did not reveal significant changes in transcript levels in CGN$^{-/-}$ mouse tissues. This could be due not only to the ability of mouse embryonic and adult tissues to adapt to and compensate for the effects of CGN knockout, but also, in part, to the heterogeneity in cell composition of the tissues we analyzed. In contrast, claudin-2 protein expression was increased in the kidney and duodenum tissues of CGN$^{-/-}$ mice, confirming previous observations on embryoid bodies and MDCK cells (Guillemot et al., 2004; Guillemot and Citi, 2006). Importantly, increased claudin-2 expression was not reflected in increased intensity of immunohistochemical labeling, similarly to what previously observed in cingulin-depleted MDCK cells (Guillemot and Citi, 2006), or in any ectopic localization of the claudin-2 signal.

Through which mechanism does CGN KO in mice result in increased claudin-2 expression? In contrast to what observed in cultured cells (Guillemot et al., 2004; Guillemot and Citi, 2006), increased claudin-2 protein levels did not correlate with increased RhoA activity, suggesting that either RhoA activation is not significantly implicated in control of claudin-2 levels in the context of duodenum and kidney tissues, or that sample heterogeneity renders it difficult to accurately measure RhoA activation in tissues. Since claudin-2 expression is increased in inflammatory bowel disease (Prasad et al., 2005; Zeissig et al., 2007; Weber et al., 2008; Schulzke et al., 2009), or following treatment of intestinal cells with cytokines (Kinugasa et al., 2000; Mankertz et al., 2009), we investigated whether increased inflammatory cytokines could be detected in the intestine of CGN$^{-/-}$ mice. However, since markers of intestinal and hepatic inflammation and cytokine levels were not altered, the increased claudin-2 expression in the duodenum is not a consequence of either inflammation or increased cytokine signaling.

Another important question is whether the twofold increase in claudin-2 protein levels might have any functional consequences on the permeability barrier properties of the kidney and duodenum. Claudin-2 forms cation-selective pores, and is typical of leaky, water-transporting epithelia, such as the kidney proximal tubule (Furuse et al., 2001; Kiuchi-Saishin et al., 2002). Isolated kidney proximal tubules from claudin-2 knockout mice show a decreased transepithelial reabsorption of $Na^+$ and $Cl^-$ and water, although the structure of TJ and the tubular excretion of $Na^+$ and $Cl^-$ ions in claudin-2 KO mice is normal (Muto et al., 2010). Ectopic overexpression of claudin-2 in kidney cells, which lack claudin-2 (MDCK-I and MDCK-C7), results in a conversion of TJ from 'tight' to 'leaky' (Furuse et al., 2001; Amasheh et al., 2002). However, overexpression of claudin-2 in CGN-depleted MDCK-II cells (which express claudin-2) does not result in altered ionic permeability (Guillemot and Citi, 2006). Since the immunohistochemical localization of claudin-2 in kidney and duodenum sections from CGN$^{-/-}$ and CGN$^{+/+}$ mice was indistinguishable, we conclude that the increased expression of claudin-2 in CGN$^{-/-}$ tissues occurs in the same cell types where claudin-2 is normally expressed, and not ectopically. Thus, although future studies are required to study in detail the role of CGN in kidney and intestine physiology and pathophysiology, our results and past observations together indicate that the increase in claudin-2 expression in CGN$^{-/-}$ tissues is unlikely to affect their ionic barrier properties. It is noteworthy that when claudin-2 upregulation in human intestine has been correlated with increased mucosa permeability, such as in the colon of patients with inflammatory bowel disease, the increase in claudin-2 expression was quantitatively much higher, and was in a context of inflammation, increased cytokine activity, and disorganized mucosal architecture (Prasad et al., 2005; Zeissig et al., 2007; Weber et al., 2008; Schulzke et al., 2009). Since the histology of CGN$^{-/-}$ intestines was normal, and no marker of inflammation was altered in CGN$^{-/-}$ mice, our work suggests that the approximate twofold increase in claudin-2 polypeptide alone is not sufficient to induce inflammation or barrier leakage in the intestine.

We tested whether acute injury models targeting the intestinal mucosa would elicit different responses in CGN$^{+/+}$ and CGN$^{-/-}$ mice. The clinical symptoms and levels of inflammation markers were similar in CGN$^{+/+}$ and CGN$^{-/-}$ littermates, when challenged by the administration of dextran sodium sulfate, a model of acute injury of the colon. In contrast, using the cysteamine model of duodenal ulcer induction, CGN$^{-/-}$ mice showed a significantly higher ulcer index than CGN$^{+/+}$ mice, due to an increase in ulcer number, score, and prevalence. These results suggest that the lack of cingulin either renders the duodenal mucosa more sensitive to the ulcerogenic action of cysteamine, or it reduces the ability of the epithelium to repair

itself. These hypotheses, and the potential role of claudin-2 in this phenotype, should be investigated by future studies. Cysteamine induces ulcers through multiple, complex mechanisms, including acid hypersecretion, and modulation of mucosal enzymes, local and systemic neurotransmitters, and hormones, such as histamine and gastrin (Szabo et al., 1979; Boesby et al., 1983). Repair mechanisms after injury include epithelial restitution, a process that rapidly reseals superficial wounds in the intestinal tract, and proliferation and differentiation of epithelial cells (Moore et al., 1989; Sturm and Dignass, 2008). Our results, showing no significant difference in the proliferation rates of intestinal cells, either under normal conditions or after administration of cysteamine, suggest that different proliferation rates are not mechanistically implicated in the different pathophysiological response of $CGN^{+/+}$ and $CGN^{-/-}$ mice.

In conclusion, our results show that at the whole organism level cingulin is dispensable for the structure and function of TJ, and plays a role in regulating claudin-2 expression in selected epithelial organs, and the response of the duodenal mucosa to the ulcerogenic injury of cysteamine. This is to our knowledge the first reported evidence that knockout of a junctional protein influences ulcer formation *in vivo*, and that TJ may be implicated in ulcer pathogenesis.

One possible explanation for the milder gene expression and RhoA activation phenotype of $CGN^{-/-}$ mice with respect to embryoid bodies and MDCK cells is that redundant proteins and mechanisms may compensate for the lack of cingulin. One candidate is paracingulin (CGNL1/JACOP), a protein that is structurally related to CGN, and has partially overlapping functions with CGN in cultured cells (Ohnishi et al., 2004; Guillemot et al., 2008a; Paschoud et al., 2011; Paschoud et al., 2012). Although paracingulin expression was not increased in $CGN^{-/-}$ tissues, suggesting no compensatory upregulation, it will be interesting to analyze the phenotype of $CGNL1^{-/-}$ mice, and double $CGN^{-/-}$/$CGNL1^{-/-}$ mice, to address in further detail the physiological roles of these related proteins in a whole organism.

## Materials and Methods

### Construction of the cingulin targeting vector

Genomic DNA fragments of the mouse cingulin (CGN) locus were isolated from a 129SvJ library (Guillemot et al., 2004). The targeting vector (TV-CGN-3LoxP) was obtained by cloning a *Kpn*I–*Eco*RV fragment comprising exons 1-4 into pBluescriptSK(-), lacking the *Xba*I site. A neomycin resistance cassette flanked by LoxP and *Xba*I sites was inserted into the *Xba*I site between exons 1 and 2. This construct was excised from the vector by digestion with *Kpn*I/*Not*I, and ligated with the *Xho*I–*Kpn*I genomic fragment upstream of exon 1 (Fig. 1), in a pSK- vector (cut with *Xho*I–*Not*I) lacking the *Kpn*I site. An oligonucleotide containing the upstream LoxP site, flanked by *Kpn*I and *Eco*RI on the 5′ side, and *Kpn*I on the 3′ side, was cloned into the *Kpn*I site upstream of exon 1. The targeting vector was linearized by *Not*I digestion prior to transfection into 129SvJ ES cells. Selection of neo-resistant clones, and preparation of lysates for genotyping was carried out by InGenious Targeting Laboratory (Stony Brook, NY, USA).

### Genotyping by Southern blotting and RT-PCR, and generation of $CGN^{-/-}$ mice

Genomic DNA samples from neo-resistant ES cell clones ($n$=288) were analyzed by Southern blot analysis, using 3′ and 5′ probes labeled by the DIG High Prime kit (Roche, Switzerland). The 5′ probe was a 295 bp *Sac*II–*Xho*I genomic fragment upstream of the *Xho*I site. The 3′ probe was a 727 bp fragment (amplified by PCR using primers 5′-AGATTTCTCTCCCATACATATATAT-3′ (forward) and 5′-ATTATTGCAGGCTTGGCAGGG-3′ (reverse), which comprised exon 6 (Fig. 1). The Neo cassette probe was PCR amplified using primers 5′-ATGGGATCGG-CCATTGAACAAG-3′ (forward) and 5′-TCAGAAGAACTCGTCAAGAAGG-3′ (reverse). Positive ES cell clones were injected into C57BL/6 blastocysts, to generate chimeras. Genomic DNA was analyzed by PCR using primers (Fig. 1). (a): 5′-GTTATCTGTGTAAGGAGTGTGA-3′ (forward); (b): 5′-GGTGATGTCTCTAG-GGTAAGG-3′ (reverse); (c): 5′-GCACCTTTCATAATGCAGGCT-3′ (forward); (d): 5′-GGAATGCTTCAGGCCTGAGG-3′ (reverse). Blastocyst injection, generation of chimeras and mating to the WT strain was carried out by InGenious Targeting Laboratory.

Heterozygous mice containing one targeted cingulin allele (F1) were mated to MeuCre40 mice (Leneuve et al., 2003) (from Prof. Holzenberger, INSERM, Paris, France) to generate mosaic mice (F2) harboring the Cre recombinase. Mosaic mice were mated to WT C57BL/6 mice, and the offspring (F3) was genotyped by PCR, (primer sets shown in Fig. 1C), to identify ‘true’ heterozygous mice, that contained the mutated allele ($CGN^{+/-}$) without the Neo cassette. Heterozygous mice were crossed to WT C57BL/6 mice, to obtain mice containing the mutated allele, but lacking the Cre recombinase (Cre recombinase-specific primers forward: 5′-CCTGGAAAATGCTTCTGTCCG-3′; reverse: 5′-CAGGGTGTTATAAGCAAT-CCC-3′, that amplify a 400 bp product). Finally, $CGN^{-/-}$ mice were backcrossed into WT C57BL/6 strain for nine generations, to homogenize the genetic background of WT and KO animals.

### Histology, immunohistochemistry and immunofluorescence

For histology and immunohistochemistry, formalin fixed tissues were included in paraffin, and sections processed by standard procedures. Antigen retrieval for immunohistochemistry was by citrate or EDTA buffers, followed by blocking of endogenous peroxidases. The Dako Envision+ System-HRP labeled Polymer Detection system (Dako, Baar, Switzerland) used either 3,3′-diaminobenzidinetetrahydrochloride (DAB) or 3-amino-9-ethylcarbazole (AEC) as chromogenic substrates. Sections were counterstained with Hematoxylin and Eosin. Primary antibodies for immunohistochemistry were: cingulin (Invitrogen 37-4300; 1:30), paracingulin (Invitrogen 39-8900; 1:15), claudin-5 (Invitrogen 34-1600; 1:25), claudin-7 (Invitrogen 34-9100; 1:25), claudin-1 (Invitrogen 71-7800; 1:20), phospho-histone H3 (Ser-10) (Upstate 06-570; 1:200). Proliferation rates were expressed either as percentage of positive cells (cysteamine-treated duodenum) after counting a minimum of 10 HPF (high power fields) or as number of positive cells/crypt (untreated colon and duodenum).

For immunofluorescence, tissues were embedded in Tissue-Tek, and snap frozen in liquid nitrogen-cooled isopentane. Cryostat sections (5 μm) were dried onto SuperFrost Plus slides, fixed in acetone (−20℃), and stained with: cingulin (Invitrogen 37-4300; 1:30), ZO-1 (R40-76, a gift of D. Goodenough, Harvard University; 1:50), occludin (Invitrogen 71-1500; 1:30). Secondary antibodies were labeled with either FITC or TRITC (Jackson ImmunoResearch Europe, Newmarket, UK) (Guillemot et al., 2004). Sections mounted with Prolong Antifade kit (Invitrogen) were imaged using a Zeiss LSM-510 Meta confocal microscope.

### Electron microscopy

Formalin-fixed, paraffin-embedded tissue was deparaffinized, post-fixed in osmium, and processed and embedded in EPON, according to standard procedures. Sections were stained with uranyl acetate and lead citrate, and examined with a Philips CM10 electron microscope.

### Microarray analysis and real-time quantitative reverse-transcription PCR

Total RNA was isolated from scraped intestinal cells of age-matched pairs of $CGN^{+/+}$ and $CGN^{-/-}$ littermates ($n$=3), using the RNeasy mini kit (Qiagen, Basel, Switzerland). 500 ng was amplified and labeled using the Illumina TotalPrep RNA Amplification kit (Ambion, Rotkreuz, Switzerland). RNA and cRNA quality was assessed by capillary electrophoresis on Agilent 2100 Bioanalyzer. Hybridization on Illumina mouse-6_v1_1_11234304 expression arrays was carried out according to the manufacturer’s instructions. Data were normalized and analyzed using Illumina Beadstudio 3.1.3 (background correction and quantile normalization). Expression profiles of each sample were imported into Partek Genomics Suite (Partek, USA). In addition to expression values, Illumina BeadStudio software computes a detection $P$-value. Based on this, each probe was assigned a detection flag [P (present): $P<0.045$; M (marginal): $P$ between 0.050 and 0.045; A (absent): $P>0.05$]. Expression values below a defined threshold (i.e. 20) are set to the threshold in order to remove negative values after background correction. To identify differentially expressed transcripts, $t$-test and additional steps of filtering (by fold change equal to 2) were carried out.

For real-time qRT-PCR, RNA was prepared from tissues of age-matched pairs of $CGN^{+/+}$ and $CGN^{-/-}$ littermates ($n$=4–6). cDNA preparation and RT-PCR was carried out as described previously, using the same primer sets (Guillemot et al., 2004).

### Preparation of tissue lysates and immunoblotting

Excised fragments of kidney and liver, and mucosal scrapings of intestinal epithelial cells were obtained from age-matched (10- to 16-weeks old) pairs of $CGN^{+/+}$ and $CGN^{-/-}$ littermates ($n$=6–8), and homogenized in three volumes of lysis buffer (see below). For the duodenum, ileum and colon samples, intestinal cells were scraped from 2.5 cm-long segments, distal to the gastric-duodenal junction, proximal to the cecum, and distal to the cecum, respectively. Different

lysis buffers and protocols were tested to maximise TJ protein solubilization, and the following buffers were selected: lysis buffer A (kidney): 50 mM Tris-HCl, pH 7.4, 100 mM sodium pyrophosphate, 100 mM sodium fluoride, 10 mM EDTA, 10 mM sodium orthovanadate, 2 mM PMSF, 1% Triton X-100, 1% SDS, 10 mM DTT, protease inhibitor cocktail mix (1×, Roche); lysis buffer B (duodenum, ileum, colon): 25 mM Hepes, pH 7.4, 100 mM NaCl 1% Triton X-100, 10% glycerol, 0.03% sodium azide, 1 mM PMSF, protease inhibitor cocktail mix (1×, Roche); lysis buffer C (liver): 50 mM Tris-HCl, pH 9.5, 2% SDS, 65 mM DTT, 10% glycerol. Tissues were homogenized in a dounce homogenizer at 4℃, incubated for 60 min at 4℃ (only for samples in lysis buffer B), and centrifuged at 4℃ (A: 12,000 rpm 30 min, B: 12,000 rpm 15 min, C: 45,000 rpm 2 hr).

For immunoblotting, nitrocellulose sheets were blocked in TBS-milk (150 mM NaCl, 50 mM Tris-HCl pH 7.5, 0.1% Tween-20, 5% skimmed milk) for 1 hr, and incubated with the following antibodies: cingulin (Invitrogen 3644-01, 1:500; Invitrogen 37-4300 1:2500), paracingulin (rabbit 20896 1:10,000, Invitrogen 39-8900, 1:500), ZO-1 (Invitrogen 61-73000, 1:2000), ZO-3 (rabbit serum, from Dr K. Matter, University College, London, 1:200), claudin-2 (Invitrogen 32-5600; 1:250), occludin (Invitrogen 33-1500, 1:500), RhoA (Santa Cruz sc-179, 1:200), followed by HRP-labeled secondary antibodies, and chemiluminescent revelation. Protein loadings were adjusted to normalize β-tubulin content. For quantitative evaluation of protein levels, autoradiograms from pairs of WT/KO littermates were analyzed with the Bio-Rad QuantityOne software. For each couple, values of WT littermates were taken as 100%, and values of KO mice were expressed as percent of WT. Data were expressed as mean of percentage values.

#### Measurement of RhoA activity

The mucosa was scraped off the intestinal segment, lysed in 0.5 ml MLB buffer (150 mM NaCl, 25 mM Hepes, pH 7.5, 1% NP-40, 10 mM $MgCl_2$, 1 mM EDTA, 10% glycerol, 25 mM NaF, 1 mM sodium orthovanadate, 0.1 mM PMSF, 1× Roche protease inhibitor cocktail) at 4℃, incubated for 15 min at 4℃ shaking, and centrifuged 10 min at 14,000 rpm, at 4℃. The supernatants were analyzed by SDS-PAGE and immunoblotting to normalize total RhoA levels, and equivalent amounts of lysates were incubated with GST–rhotekin/Rho-binding domain (RBD) bound to glutathione–Sepharose4B beads, to isolate the active RhoA fraction (Guillemot and Citi, 2006).

#### Measurement of intestinal barrier function and inflammation

Mucosal preparations from duodenum and colon of age-matched pairs (12–16 weeks) of $CGN^{+/+}$ and $CGN^{-/-}$ littermates were mounted in Ussing chambers, and the electrical resistance ($R$; $\Omega/cm^2$) was measured (Brun et al., 2007). Endotoxin levels in sera collected from the portal vein were measured using an ELISA assay (Brun et al., 2007). The genotype of the mice was unknown to the experimenter until completion of the experiment, to eliminate any experimenter bias.

Inflammation was assessed histologically on Hematoxylin- and Eosin-stained sections, and by measurement of systemic TNF-α levels, myeloperoxidase (MPO) activity and pro-inflammatory protein levels (TNF-α and IL-1β) (Brun et al., 2007). Activation of hepatic stellate cells (HSCs) isolated from liver was determined by measurement of fold-induction of mRNA expression by LPS (as determined by qRT-PCR) of fibronectin, collagen type I, monocyte chemoattractant protein 1 (MCP-1) (Brun et al., 2005; Brun et al., 2007).

Acute intestinal injury and inflammation was induced by administering water containing 3% w/vol dextran sodium sulfate (DSS) for 6 days. Animal body weight, stool consistency and presence of fecal blood were recorded daily. Colon samples were either fixed in paraformaldehyde for histological examination, or snap frozen, for evaluation of MPO activity, and measurement of IL-1β and TNF-α levels. Experiments and protocols on mice were authorized by the University of Padova Ethics Committee for animal experimentation.

#### Cysteamine model of ulcer induction

Chemically induced duodenal ulcers (Szabo, 1978; Cahill et al., 1986) were produced by a single oral administration of cysteamine hydrochloride (175 μg/g), to $CGN^{+/+}$ and $CGN^{-/-}$ littermates (age 12–16 weeks) that had been reared in the same animal facility room, and had undistinguishable health status. In preliminary experiments, a dose-effect curve on WT mice selected the dose of 175 μg/g (mouse weight) as the minimum effective dose required to induce typical ulcer lesions without mortality in WT mice, within a 9 hr period. The mice genotype was unknown to the experimenter until completion of the experiment, to eliminate any experimenter bias. Mice were sacrificed within 9 hr after administration of cysteamine, or at earlier times, if they showed signs of distress. The duodenum was dissected for macroscopic examination and histopathological analysis. The number of duodenal ulcers was counted, and each ulcer was given a severity score (Szabo, 1978): 0=no ulcer, 1=superficial ulcer, 2=deep ulcer, 3=perforation. Ulcer index was measured for each mouse ($n$=12) using the following formula (Vogel and Vogel, 1997): $U_I=U_N+U_S+U_P\times10^{-1}$, where $U_I$ is ulcer index, $U_N$ is ulcer number, $U_S$ is ulcer score, and $U_P$ is ulcer prevalence (percentage of animals with ulcers). The average ulcer index with standard deviation was plotted for each genotype.

#### Statistical analysis

All quantitative data were expressed as means ± standard deviation. Comparisons were drawn between groups for parametric data using Student's $t$-test (unpaired, two-tailed). Results were considered statistically significant when $P<0.05$.


## Acknowledgements

We thank Patrizia Gindre, Nathalie Lin Marq, Lara Lunghi and Philippe Henchoz for assistance with immunohistochemistry and electron microscopy, Christian Kaister and Jeff Stutz for help with plasmid construction and RT-PCR analysis, and Olivier Schaad (Genomics Platform of the NCCR Program 'Frontiers in Genetics') for microarray analysis and statistics. Thanks also to colleagues cited in the text, for their generous gifts of reagents and materials.

## Funding

This work was supported by the State of Geneva; the Section of Biology of the University of Geneva; grants from the Swiss National Science Foundation [grant numbers 3100-052903, 3100-064089, 31003A103637 and 31003A116763 to S.C.]; the European Society of Clinical Microbiology and Infectious Diseases (ESCMID) [grant number AZMAT03031159 to P.B.]; and from the Italian Ministry of University and Research (MIUR) [grant number 2009HLNNRL_002 to I.C.].

Supplementary material available online at
http://jcs.biologists.org/lookup/suppl/doi:10.1242/jcs.101261/-/DC1


## References


**Adachi, M., Inoko, A., Hata, M., Furuse, K., Umeda, K., Itoh, M. and Tsukita, S.** (2006). Normal establishment of epithelial tight junctions in mice and cultured cells lacking expression of ZO-3, a tight-junction MAGUK protein. *Mol. Cell. Biol.* **26**, 9003-9015.

**Aijaz, S., D'Atri, F., Citi, S., Balda, M. S. and Matter, K.** (2005). Binding of GEF-H1 to the tight junction-associated adaptor cingulin results in inhibition of Rho signaling and G1/S phase transition. *Dev. Cell* **8**, 777-786.

**Amasheh, S., Meiri, N., Gitter, A. H., Schöneberg, T., Mankertz, J., Schulzke, J. D. and Fromm, M.** (2002). Claudin-2 expression induces cation-selective channels in tight junctions of epithelial cells. *J. Cell Sci.* **115**, 4969-4976.

**Boesby, S., Man, W. K., Mendez-Diaz, R. and Spencer, J.** (1983). Effect of cysteamine on gastroduodenal mucosal histamine in rat. *Gut* **24**, 935-939.

**Brun, P., Castagliuolo, I., Pinzani, M., Palù, G. and Martines, D.** (2005). Exposure to bacterial cell wall products triggers an inflammatory phenotype in hepatic stellate cells. *Am. J. Physiol. Gastrointest. Liver Physiol.* **289**, G571-G578.

**Brun, P., Castagliuolo, I., Di Leo, V., Buda, A., Pinzani, M., Palù, G. and Martines, D.** (2007). Increased intestinal permeability in obese mice: new evidence in the pathogenesis of nonalcoholic steatohepatitis. *Am. J. Physiol. Gastrointest. Liver Physiol.* **292**, G518-G525.

**Cahill, M. C., Gallagher, G. T. and Szabo, S.** (1986). Cysteamine induces duodenal ulcer in the mouse. *Digestion* **34**, 1-8.

**Citi, S., Sabanay, H., Jakes, R., Geiger, B. and Kendrick-Jones, J.** (1988). Cingulin, a new peripheral component of tight junctions. *Nature* **333**, 272-276.

**Citi, S., Sabanay, H., Kendrick-Jones, J. and Geiger, B.** (1989). Cingulin: characterization and localization. *J. Cell Sci.* **93**, 107-122.

**Citi, S., Paschoud, S., Pulimeno, P., Timolati, F., De Robertis, F., Jond, L. and Guillemot, L.** (2009). The tight junction protein cingulin regulates gene expression and RhoA signaling. *Ann. N. Y. Acad. Sci.* **1165**, 88-98.

**Citi, S., Spadaro, D., Schneider, Y., Stutz, J. and Pulimeno, P.** (2011). Regulation of small GTPases at epithelial cell-cell junctions. *Mol. Membr. Biol.* **28**, 427-444.

**Cordenonsi, M., D'Atri, F., Hammar, E., Parry, D. A., Kendrick-Jones, J., Shore, D. and Citi, S.** (1999). Cingulin contains globular and coiled-coil domains and interacts with ZO-1, ZO-2, ZO-3, and myosin. *J. Cell Biol.* **147**, 1569-1582.

**D'Atri, F., Nadalutti, F. and Citi, S.** (2002). Evidence for a functional interaction between cingulin and ZO-1 in cultured cells. *J. Biol. Chem.* **277**, 27757-27764.

**Furuse, M., Furuse, K., Sasaki, H. and Tsukita, S.** (2001). Conversion of zonulae occludentes from tight to leaky strand type by introducing claudin-2 into Madin-Darby canine kidney I cells. *J. Cell Biol.* **153**, 263-272.

**Guillemot, L. and Citi, S.** (2006). Cingulin regulates claudin-2 expression and cell proliferation through the small GTPase RhoA. *Mol. Biol. Cell* **17**, 3569-3577.

**Guillemot, L., Hammar, E., Kaister, C., Ritz, J., Caille, D., Jond, L., Bauer, C., Meda, P. and Citi, S.** (2004). Disruption of the cingulin gene does not prevent tight junction formation but alters gene expression. *J. Cell Sci.* **117**, 5245-5256.

**Guillemot, L., Paschoud, S., Jond, L., Foglia, A. and Citi, S.** (2008a). Paracingulin regulates the activity of Rac1 and RhoA GTPases by recruiting Tiam1 and GEF-H1 to epithelial junctions. *Mol. Biol. Cell* **19**, 4442-4453.

**Guillemot, L., Paschoud, S., Pulimeno, P., Foglia, A. and Citi, S.** (2008b). The cytoplasmic plaque of tight junctions: a scaffolding and signalling center. *Biochim. Biophys. Acta* **1778**, 601-613.

**Ikeda, W., Nakanishi, H., Miyoshi, J., Mandai, K., Ishizaki, H., Tanaka, M., Togawa, A., Takahashi, K., Nishioka, H., Yoshida, H. et al.** (1999). Afadin: A key molecule essential for structural organization of cell-cell junctions of polarized epithelia during embryogenesis. *J. Cell Biol.* **146**, 1117-1132.

**Katsuno, T., Umeda, K., Matsui, T., Hata, M., Tamura, A., Itoh, M., Takeuchi, K., Fujimori, T., Nabeshima, Y. I., Noda, T. et al.** (2008). Deficiency of zonula occludens-1 causes embryonic lethal phenotype associated with defected yolk sac angiogenesis and apoptosis of embryonic cells. *Mol. Biol. Cell* **19**, 2465-2475.

**Kinugasa, T., Sakaguchi, T., Gu, X. and Reinecker, H. C.** (2000). Claudins regulate the intestinal barrier in response to immune mediators. *Gastroenterology* **118**, 1001-1011.

**Kiuchi-Saishin, Y., Gotoh, S., Furuse, M., Takasuga, A., Tano, Y. and Tsukita, S.** (2002). Differential expression patterns of claudins, tight junction membrane proteins, in mouse nephron segments. *J. Am. Soc. Nephrol.* **13**, 875-886.

**Leneuve, P., Colnot, S., Hamard, G., Francis, F., Niwa-Kawakita, M., Giovannini, M. and Holzenberger, M.** (2003). Cre-mediated germline mosaicism: a new transgenic mouse for the selective removal of residual markers from tri-lox conditional alleles. *Nucleic Acids Res.* **31**, e21.

**Mankertz, J., Amasheh, M., Krug, S. M., Fromm, A., Amasheh, S., Hillenbrand, B., Tavalali, S., Fromm, M. and Schulzke, J. D.** (2009). TNFalpha up-regulates claudin-2 expression in epithelial HT-29/B6 cells via phosphatidylinositol-3-kinase signaling. *Cell Tissue Res.* **336**, 67-77.

**McCrea, P. D., Gu, D. and Balda, M. S.** (2009). Junctional music that the nucleus hears: cell-cell contact signaling and the modulation of gene activity. *Cold Spring Harb. Perspect. Biol.* **1**, a002923.

**Mitic, L. L. and Anderson, J. M.** (1998). Molecular architecture of tight junctions. *Annu. Rev. Physiol.* **60**, 121-142.

**Moore, R., Carlson, S. and Madara, J. L.** (1989). Rapid barrier restitution in an in vitro model of intestinal epithelial injury. *Lab. Invest.* **60**, 237-244.

**Muto, S., Hata, M., Taniguchi, J., Tsuruoka, S., Moriwaki, K., Saitou, M., Furuse, K., Sasaki, H., Fujimura, A., Imai, M. et al.** (2010). Claudin-2-deficient mice are defective in the leaky and cation-selective paracellular permeability properties of renal proximal tubules. *Proc. Natl. Acad. Sci. USA* **107**, 8011-8016.

**Ohnishi, H., Nakahara, T., Furuse, K., Sasaki, H., Tsukita, S. and Furuse, M.** (2004). JACOP, a novel plaque protein localizing at the apical junctional complex with sequence similarity to cingulin. *J. Biol. Chem.* **279**, 46014-46022.

**Okayasu, I., Hatakeyama, S., Yamada, M., Ohkusa, T., Inagaki, Y. and Nakaya, R.** (1990). A novel method in the induction of reliable experimental acute and chronic ulcerative colitis in mice. *Gastroenterology* **98**, 694-702.

**Paschoud, S. and Citi, S.** (2008). Inducible overexpression of cingulin in stably transfected MDCK cells does not affect tight junction organization and gene expression. *Mol. Membr. Biol.* **25**, 1-13.

**Paschoud, S., Yu, D., Pulimeno, P., Jond, L., Turner, J. R. and Citi, S.** (2011). Cingulin and paracingulin show similar dynamic behaviour, but are recruited independently to junctions. *Mol. Membr. Biol.* **28**, 123-135.

**Paschoud, S., Guillemot, L. and Citi, S.** (2012). Distinct domains of paracingulin are involved in its targeting to the actin cytoskeleton and regulation of apical junction assembly. *J. Biol. Chem.* **287**, 13159-13169.

**Prasad, S., Mingrino, R., Kaukinen, K., Hayes, K. L., Powell, R. M., MacDonald, T. T. and Collins, J. E.** (2005). Inflammatory processes have differential effects on claudins 2, 3 and 4 in colonic epithelial cells. *Lab. Invest.* **85**, 1139-1162.

**Rahner, C., Mitic, L. L. and Anderson, J. M.** (2001). Heterogeneity in expression and subcellular localization of claudins 2, 3, 4, and 5 in the rat liver, pancreas, and gut. *Gastroenterology* **120**, 411-422.

**Schmitz, H., Barmeyer, C., Fromm, M., Runkel, N., Foss, H. D., Bentzel, C. J., Riecken, E. O. and Schulzke, J. D.** (1999). Altered tight junction structure contributes to the impaired epithelial barrier function in ulcerative colitis. *Gastroenterology* **116**, 301-309.

**Schulzke, J. D., Ploeger, S., Amasheh, M., Fromm, A., Zeissig, S., Troeger, H., Richter, J., Bojarski, C., Schumann, M. and Fromm, M.** (2009). Epithelial tight junctions in intestinal inflammation. *Ann. N. Y. Acad. Sci.* **1165**, 294-300.

**Shin, K., Fogg, V. C. and Margolis, B.** (2006). Tight junctions and cell polarity. *Annu. Rev. Cell Dev. Biol.* **22**, 207-235.

**Simon, D. B., Lu, Y., Choate, K. A., Velazquez, H., Al-Sabban, E., Praga, M., Casari, G., Bettinelli, A., Colussi, G., Rodriguez-Soriano, J. et al.** (1999). Paracellin-1, a renal tight junction protein required for paracellular Mg2+ resorption. *Science* **285**, 103-106.

**Sturm, A. and Dignass, A. U.** (2008). Epithelial restitution and wound healing in inflammatory bowel disease. *World J. Gastroenterol.* **14**, 348-353.

**Szabo, S.** (1978). Duodenal ulcer disease. Animal model: cysteamine-induced acute and chronic duodenal ulcer in the rat. *Am. J. Pathol.* **93**, 273-276.

**Szabo, S., Haith, L. R., Jr and Reynolds, E. S.** (1979). Pathogenesis of duodenal ulceration produced by cysteamine or propionitrile: influence of vagotomy, sympathectomy, histamine depletion, H-2 receptor antagonists and hormones. *Dig. Dis. Sci.* **24**, 471-477.

**Tsukita, S. and Furuse, M.** (2000). Pores in the wall: claudins constitute tight junction strands containing aqueous pores. *J. Cell Biol.* **149**, 13-16.

**Turner, J. R.** (2000). 'Putting the squeeze' on the tight junction: understanding cytoskeletal regulation. *Semin. Cell Dev. Biol.* **11**, 301-308.

**Van Itallie, C. M. and Anderson, J. M.** (2006). Claudins and epithelial paracellular transport. *Annu. Rev. Physiol.* **68**, 403-429.

**Vogel, H. G. and Vogel, W. H.** (1997). Anti-ulcer activity. In *Drug Discovery and Evaluation: Pharmacological Assays* (ed. H. G. Vogel and W. H. Vogel), pp. 486-491. Berlin, DE: Springer-Verlag.

**Weber, C. R., Nalle, S. C., Tretiakova, M., Rubin, D. T. and Turner, J. R.** (2008). Claudin-1 and claudin-2 expression is elevated in inflammatory bowel disease and may contribute to early neoplastic transformation. *Lab. Invest.* **88**, 1110-1120.

**Xu, J., Kausalya, P. J., Phua, D. C., Ali, S. M., Hossain, Z. and Hunziker, W.** (2008). Early embryonic lethality of mice lacking ZO-2, but Not ZO-3, reveals critical and nonredundant roles for individual zonula occludens proteins in mammalian development. *Mol. Cell. Biol.* **28**, 1669-1678.

**Xu, J., Anuar, F., Ali, S. M., Ng, M. Y., Phua, D. C. and Hunziker, W.** (2009). Zona occludens-2 is critical for blood-testis barrier integrity and male fertility. *Mol. Biol. Cell* **20**, 4268-4277.

**Zeissig, S., Bürgel, N., Günzel, D., Richter, J., Mankertz, J., Wahnschaffe, U., Kroesen, A. J., Zeitz, M., Fromm, M. and Schulzke, J. D.** (2007). Changes in expression and distribution of claudin 2, 5 and 8 lead to discontinuous tight junctions and barrier dysfunction in active Crohn's disease. *Gut* **56**, 61-72.

**Zhadanov, A. B., Provance, D. W., Jr, Speer, C. A., Coffin, J. D., Goss, D., Blixt, J. A., Reichert, C. M. and Mercer, J. A.** (1999). Absence of the tight junctional protein AF-6 disrupts epithelial cell-cell junctions and cell polarity during mouse development. *Curr. Biol.* **9**, 880-888.